Registration Assisted Image Smoothing and Segmentation

B.C. Vemuri[1], Y. Chen[2], and Z. Wang[1]

[1] Department of CISE, University of Florida
Gainesville, Fl. 32611
vemuri|zwang@cise.ufl.edu
[2] Department of Mathematics, University of Florida
Gainesville, Fl. 32611 yun@math.ufl.edu

Abstract. Image segmentation is a fundamental problem in Image Processing, Computer Vision and Medical Imaging with numerous applications. In this paper, we address the atlas-based image segmentation problem which involves registration of the atlas to the subject or target image in order to achieve the segmentation of the target image. Thus, the target image is segmented with the assistance of a registration process. We present a novel variational formulation of this registration assisted image segmentation problem which leads to solving a coupled set of nonlinear PDEs that are solved using efficient numerical schemes. Our work is a departure from earlier methods in that we have a *unified variational principle* wherein registration and segmentation are simultaneously achieved. We present several 2D examples on synthetic and real data sets along with quantitative accuracy estimates of the registration.

1 Introduction

Segmentation of noisy image data is fundamental to the fields of Computer Vision and Image Processing. There are numerous existing methods in literature for achieving this goal. In Medical Imaging applications, segmentation can be a daunting task due to possibly large inhomogeneities in image intensities across an image e.g., in MR images. These inhomogeneities combined with volume averaging during the imaging and possible lack of precisely defined shape boundaries for certain anatomical structures complicates the segmentation problem immensely. One possible solution for such situations is atlas-based segmentation where the atlas is a given ground-truth segmentation. The atlas can be constructed in various ways and it allows one to incorporate prior information about the anatomical structure of interest and this information can be input from one or more experts. The atlas once constructed can be used as a template and can be registered non-rigidly to the image being segmented (henceforth called a target image) thereby achieving the desired segmentation. This approach has been quite popular in the recent past for segmenting cortical and sub-cortical structures in the human brain from MRI images. We will now briefly review some of these approaches in the following. Note that the atlas-based registration problem assumes that

A. Heyden et al. (Eds.): ECCV 2002, LNCS 2353, pp. 546–559, 2002.

the ground truth segmentation is given and requires the subject/target image be segmented using the information in the atlas. Assuming a given atlas i.e., segmented source image is the only way to solve this problem since, the shape of interest in the source image for our application is at times not well defined in terms of having well defined contrast boundaries at any scale. Approaches that try to simultaneously achieve segmentation of the shape of interest in both the source and target images as in [1,11] are unsuitable for such problems because, the source shape must be learnt over a population of pre-identified shapes where the pre-identification is achieved with the aid of an expert. The reader is however warned that in this paper, we have not included examples where the atlas was obtained via a rigorous training process. However, our research is well poised to proceed in this direction with the acquisition of such population of shapes in the case of a hippocampus in the human brain. The data ground truth shape acquisition for a reasonable number of data sets with the aid of an expert is quite tedious and should not be underestimated.

1.1 Previous Work: Brief Review

Many of the methods that achieve atlas-based segmentation are based on estimating the non-rigid deformation field between the atlas image and the target image and then applying the estimated deformation field to the desired shape in the atlas to achieve the segmentation of the corresponding structure in the target/subject image. In the following, we will briefly review some of these methods.

In Chen et.al., [3], an atlas-based segmentation scheme is described that uses expert input to define the atlas and then warp it to the subject brain MRI to segment the subject brain which is then followed by morphometrics. The coordinate warp was determined using the popular sum of squared differences (SSD) measure defined over the image pair intensity functions. The warp was computed only at the control points and interpolated elsewhere using B-spline basis, thus accruing computational savings because the number of control points is dramatically smaller than the original grid points. The vector field describing the coordinate warp was then improved using a simple but ad-hoc heuristic iterative improvement technique. The computed vector field was then used to warp the given segmentation in the source image on to the target image. The governing equations in this iterative improvement are almost identical to the non-rigid deformation estimation equations reported in Dawant et.al., [6] which are in turn identical to the governing equation of non-rigid registration in Thirion [19]. All these methods are not strictly derived from a variational principle and hence can not be interpreted as minimizers of any cost functionals. Moreover, they do not achieve registration and segmentation simultaneously in a unified mathematical framework.

Among the image registration methods, one popular approach is based on maximizing mutual information reported simultaneously in Viola and Wells [22] and Collignon *et al.* [5]. Mutual information between the model and the image

that are to be registered is maximized using a stochastic analog of the gradient descent method. Impressive experiments have been reported using this scheme for rigid as well as non-rigid registration **[9,13,18]**. Recently, MI-based non-rigid registration methods have been used in [7] for constructing statistical deformation models. These models are then used in constructing atlases along with information about the variability in the population used for constructing the atlas. Once again, these methods do not use a unified framework for registration and segmentation but instead they first estimate the deformation field and then apply it to the atlas/mask to detect the corresponding shape in the target/subject image.

Another popular non-rigid registration method that has been used in the context of achieving segmentation is based on the fluid-flow model introduced in Christensen et.al., [8]. In this approach the registration transformation is modeled by a viscous fluid flow model expressed as a partial differential equation (PDE). The model primarily describes the registration as a local deformation expressed as a fluid flow via a nonlinear PDE. In the fluid-flow based methods, the reported computational times for registration of 2D and 3D data sets on uniprocessor workstations are very large. The fastest implementation of the viscous fluid flow model by Schormann *et al.* [15] using a multi-grid scheme takes 200 mins. of CPU time on a Sparc-10 for registering two $64 \times 128 \times 128$ images. This fluid flow based non-rigid registration has been used quite widely in achieving atlas-based segmentation and we refer the reader to [23,4,10]. A more mathematically thorough treatment of the non-rigid registration which subsumes the fluid methods was presented in Trouve [20]. In his technique, the transformation between the two images is treated as a mapping an appropriate metric is defined to characterize the deviation of this map from the identity. The formulation is very interesting and yields a diffeomorphic mapping unlike most other approaches. Examples of large deformation mappings are shown for 2D synthetic images and real images of size (128,128). The method in Trouve [20] has however not been used in atlas-based segmentation. It should however undoubtedly yield segmentations that are as good as or better than those obtained using the fluid-flow model of Christensen et.al. [8].

In [2], a level-set based image registration algorithm was introduced that was designed to non-rigidly register two 3D volumes from the same modality of imaging. This algorithm was computationally efficient and was applied to achieve atlas-based segmentation. Examples of application of this non-rigid deformation estimation scheme were shown for hippocampal segmentation from human brain MRI. Although, this scheme was mathematically well grounded, the task of atlas-based segmentation was achieved in two separate stages, one in which the deformation field was determined and another where the target image was segmented via an application of the estimated deformation field to the atlas-segmentation. This is the the same two stage approach philosophy followed by earlier researchers and can be effected by a cumulation of errors from each stage and the achieved segmentation may not be very accurate. The target shape could be either under or oversegmented due to registration errors and it

is desirable to improve on this segmentation by using any available information (global/local) in the target image over and above what was used during the registration process. One possibility is to drive the warped segmentation using some type of active modeling framework which would use the warped segmentation as an initialization. This might possibly yield the desired solution but the approach itself would be a combination of two disjoint approaches. Instead, in this paper, we present a novel variational formulation of this registration assisted image segmentation problem which leads to solving a coupled set of nonlinear PDEs that are solved using very efficient numerical schemes. In this framework, the registration of the template with the target image and the segmentation of the desired shape from the target image are simultaneously achieved by solving the coupled PDEs. We present several 2D examples on synthetic and real data sets.

The rest of the paper is organized as follows: In section 2, we present the mathematical model for achieving the simultaneous registration and segmentation as well as the numerical algorithm used in the minimization. Section 4 contains several examples of algorithm performance on 2D images. Finally, section 5 draws some conclusions.

2 Registration+Segmentation Model

Our model for registration-assisted segmentation achieves registration and segmentation in one unified framework. The problem is posed in a variational framework as a single variational principle and its solution is obtained by solving the associated Euler Lagrange equations, which are nonlinear partial differential equations (PDEs). Let $I_1(x, y)$ and $I_2(x, y)$ be the two given images and let C be the boundary or boundaries of the given segmentation (either a single closed contour or several contours) of I_1. For simplicity, we use a modified version of the SSD registration model [17] wherein the modification allows for the two image pairs being registered to differ in contrast and brightness. This measure however can be replaced by any other match metric (normalized cross-correlation etc.) in the framework proposed here, of course, the Euler-Lagrange equations need to be changed appropriately. The image segmentation aspect of our model includes an image smoothing component as in the work reported in [21]. The basic idea of the smoothing and segmentation aspect is a curve evolution form of the classical Mumford-Shah model of image smoothing and segmentation as described in [21] but with the added twist that the segmentation is dependent on the non-rigid registration between the image pairs. The variational principle describing our formulation of the registration assisted segmentation problem is given by,

$$E(v, \hat{I}_2, \alpha, \beta) = \int_{\Omega/C} \Big\{ \lambda_1 \|\nabla \hat{I}_2(v(x))\|^2 + \lambda_2 \|\hat{I}_2(v(x)) - I_2(v(x))\|^2 + \lambda_3 \|I_1(x) - \alpha * \hat{I}_2(v(x)) - \beta\|^2 \Big\} dx + \int_{\Omega} \lambda_4 \|\nabla v(x)\|^2 dx. \quad (1)$$

Here, $\hat{I}_2$ denotes the desired unknown smooth approximation to the target image, α accounts for a constant contrast variation between the two image pairs and β accounts for the brightness differences between the image pairs. The two images are assumed to be non-rigidly mis-aligned by a vector field transformation $v(x)$. Ω is the image domain in I_1. $\lambda_i, i = 1, .., 4$ are parameters that weight the importance of each term in the variational principle. At this time, we have chosen to keep the smoothing of the vector field and the image I_2 simple by using the L_2 norm which leads to computationally efficient algorithms. L_1 norm based smoothing in this context will be the focus of our future work.

Let, $\mathcal{X}_c(x)$ be a characteristic function of the curve C, i.e., $\mathcal{X}_c(x) = 0$, if $x \in C$, and $\mathcal{X}_c(x) = 1$, *otherwise*. Then, the Euler-Lagrange equation of the variational principle (1) is given by,

$$
\begin{aligned}
&\Delta\hat{I}_2(v(x)) + \lambda_2(\hat{I}_2(v(x)) - I_2(v(x))) + \lambda_3\alpha(\alpha\hat{I}_2(v(x)) + \beta - I_1) = 0 \\
&\quad \frac{\partial\hat{I}_2(v(x))}{\partial N} = 0, \quad x \in C \qquad (2) \\
&\lambda_4\Delta v_1 = \mathcal{X}_c\left\{\lambda_1\frac{\hat{I}_{2x}\hat{I}_{2xx} + \hat{I}_{2y}\hat{I}_{2xy}}{\|\nabla\hat{I}_2\|} + \lambda_2(\hat{I}_2 - I_2)(\hat{I}_{2x} - I_{2_x}) + \right. \\
&\quad \left.\lambda_3\alpha(\alpha\hat{I}_2 + \beta - I_1)\hat{I}_{2x}\right\} \\
&\lambda_4\Delta v_2 = \mathcal{X}_c\left\{\lambda_1\frac{\hat{I}_{2x}\hat{I}_{2xy} + \hat{I}_{2y}\hat{I}_{2yy}}{\|\nabla\hat{I}_2\|} + \lambda_2(\hat{I}_2 - I_2)(\hat{I}_{2y} - I_{2_y}) - \right. \\
&\quad \left.\lambda_3\alpha(\alpha\hat{I}_2 + \beta - I_1)\hat{I}_{2y}\right\} \\
&\int_{\Omega/C}(\alpha\hat{I}_2(v(x)) + \beta - I_1)\hat{I}_2 dx = 0 \\
&\int_{\Omega/C}(\alpha\hat{I}_2(v(x)) + \beta - I_1)dx = 0 \qquad (3)
\end{aligned}
$$

These equations are a coupled system of nonlinear PDEs and can be solved numerically as described in the following section.

3 Numerical Solution

Equations (2) and (3) can be solved numerically by discretizing them using the central finite differences. Since these are nonlinear PDEs, they need to be linearized and then solved. Our approach here will be somewhat different in that, we will use the PDE in (2) to solve for the smooth approximation $\hat{I}_2$. In order to solve for the vector field transformation and the parameters α and β, we will directly discretize the variational principle (1) and solve it using the nonlinear preconditioned conjugate gradient algorithm. More on this in the subsequent paragraphs. This works out to be simpler to linearize and hence justifying the approach.

The linearization of the first PDE which involves image smoothing is done by using the vector field transformation and the contrast as well as the brightness estimates obtained from the previous iteration. Once the $v(x), \alpha, \beta$ is fixed, we can compute the inverse transformation of $v(x)$ as $u(x)$, then the first PDE becomes:

$$\begin{aligned} \Delta \hat{I}_2(x) + \lambda_2 \left[\hat{I}_2(x) - I_2(x)\right] + \lambda_3 \alpha \left[\alpha \hat{I}_2(x) + \beta - I_1(u(x))\right] = 0 \\ \frac{\partial \hat{I}_2(x)}{\partial N} = 0, \quad x \in v(C) \end{aligned} \tag{4}$$

The above equation when discretized is a linear system which can be solved very efficiently using an incomplete-LU (ILU) preconditioned conjugate gradient (PCG) algorithm [14].

Once the smoothed image $\hat{I}_2$ is obtained, we solve the registration parameters v, α, β by using the discretized equation (1). We use the nonlinear preconditioned conjugate gradient with the incomplete LU preconditioning to efficiently solve the discretized variational problem.

3.1 Discrete Variational Principle

In this section, we present the details of the nonlinear PCG used in minimizing the discretized variational principle. Let $\mathbf{v}_1 \in R^n$ and $\mathbf{v}_2 \in R^n$ denote the vector fields defined on the entire image mesh of size n, corresponding to the components $v_{1,i}$ and $v_{2,i}$ at each mesh point respectively. The discretized variational principle (1) for fixed $\hat{I}_2$ denoted by $f(.)$ is given by,

$$\begin{aligned} f(\mathbf{v_1}, \mathbf{v_2}, \alpha, \beta) = & \sum_{(x_i, y_i) \in \Omega / C} \Big\{ \lambda_1 \|\nabla \hat{I}_2(x_i + v_{1,i}, y_i + v_{2,i})\|^2 \\ & + \lambda_2 \|\hat{I}_2(x_i + v_{1,i}, y_i + v_{2,i}) - I_2(x_i + v_{1,i}, y_i + v_{2,i})\|^2 \\ & + \lambda_3 \|\alpha \hat{I}_2(x_i + v_{1,i}, y_i + v_{2,i}) + \beta - I_1(x_i, y_i)\|^2 \Big\} \\ & + \sum_{(x_i, y_i) \in \Omega} \lambda_4 (v_{1x,i}^2 + v_{1y,i}^2 + v_{2x,i}^2 + v_{2y,i}^2) \end{aligned} \tag{5}$$

This functional is minimized using the nonlinear preconditioned conjugate gradient (NPCG) technique with an incomplete-LU preconditioner.

The general nonlinear preconditioned conjugate gradient method is outlined as follows [16]:

1. Solve $\mathbf{P}\mathbf{z}_0 = \mathbf{r}_0 = -f'(\mathbf{u}_0)$ and set $\mathbf{d}_0 = \mathbf{z}_0$.
2. Find γ_i that minimizes $f(\mathbf{u}_i + \gamma_i \mathbf{d}_i)$.
3. $\mathbf{u}_{i+1} = \mathbf{u}_i + \gamma_i \mathbf{d}_i$.
4. $\mathbf{r}_{i+1} = -f'(\mathbf{u}_{i+1})$. Solve $\mathbf{P}\mathbf{z}_{i+1} = \mathbf{r}_{i+1}$
5. $\eta_{i+1} = \frac{\mathbf{r}_{i+1}^T \mathbf{z}_{i+1}}{\mathbf{r}_i^T \mathbf{z}_i}$ or $\eta_{i+1} = \max\{\frac{\mathbf{r}_{i+1}^T (\mathbf{z}_{i+1} - \mathbf{z}_i)}{\mathbf{r}_i^T \mathbf{z}_i}, 0\}$.

6. $\mathbf{d}_{i+1} = \mathbf{z}_{i+1} + \eta_{i+1}\mathbf{d}_i$.
7. If $\mathbf{r}_{i+1} \simeq \mathbf{0}$, stop; else go to step 2.

Where, $\mathbf{u}_i$ is the unknown parameter vector being solved for and in our case, it consists of $(\mathbf{v}_1, \mathbf{v}_2, \alpha, \beta)$. Step 2 requires a line search method to minimize the function $f(\mathbf{u}_i + \gamma_i \mathbf{d}_i)$ at $\mathbf{u}_i$ along the direction $\mathbf{d}_i$. The Newton-Raphson method and the Secant method are two popular line search schemes to approximate the best γ_i. We employ the Newton-Raphson method in the nonlinear PCG. The Taylor series approximation of the function f up to the second-order terms is used to derive the approximate γ_i, giving

$$\gamma_i = -\frac{\mathbf{f}'(\mathbf{u}_i)\mathbf{d}_i}{\mathbf{d}_i^T \mathbf{f}''(\mathbf{u}_i)\mathbf{d}_i}. \tag{6}$$

In step 5, there are two ways for choosing η. The first is Fletcher-Reeves formula and the other is the Polak-Ribiere formula [12]. We adopt the latter since it usually converges much more quickly, although the nonlinear PCG needs to restart when $\eta = 0$. Note that $\mathbf{f}'(\mathbf{u})$ and $\mathbf{f}''(\mathbf{u})$ in this algorithm denote the gradient vector and the Hessian matrix of the function f given in Eq. (5). The following are the approximations for $\mathbf{f}'(\mathbf{u})$ and $\mathbf{f}''(\mathbf{u})$ where $\mathbf{u} \in R^{2n+2}$ and $\mathbf{u} = (\mathbf{v_1}\ \mathbf{v_2}\ \alpha\ \beta)^T$:

$$\mathbf{f}'(\mathbf{u}) = \begin{bmatrix} \mathbf{f'}_1 \\ \mathbf{f'}_2 \\ f'_\alpha \\ f'_\beta \end{bmatrix} + \lambda_4 \begin{bmatrix} \mathbf{K}_s & \mathbf{0} \\ \mathbf{0} & \mathbf{K}_s \\ \mathbf{0} & \mathbf{0} \end{bmatrix} \mathbf{u} \tag{7}$$

$$\mathbf{f}''(\mathbf{u}) = \begin{bmatrix} \mathbf{K}_{11} + \lambda_4 \mathbf{K}_s & \mathbf{K}_{12} & \mathbf{K}_{13} \\ \mathbf{K}_{12} & \mathbf{K}_{22} + \lambda_4 \mathbf{K}_s & \mathbf{K}_{23} \\ \mathbf{K}_{13}^T & \mathbf{K}_{23}^T & \mathbf{K}_{33} \end{bmatrix} \tag{8}$$

where the matrix $\mathbf{K}_s$ is the discrete Laplacian matrix obtained from the membrane smoothness constraint, the vectors $\mathbf{f}'_1$ and $\mathbf{f}'_2$ are obtained by concatenating the components $f'_{1,i}$ and $f'_{2,i}$ respectively, $\mathbf{K}_{11}$, $\mathbf{K}_{12}$ and $\mathbf{K}_{22}$ are all diagonal matrices with the i-th diagonal entries $K_{11,i}$, $K_{12,i}$ and $K_{22,i}$ respectively, The components $f'_{1,i}$, $f'_{2,i}$, $K_{11,i}$, $K_{12,i}$ and $K_{22,i}$ corresponding to the i-th $(1 \le i \le n)$ location are defined as:

$$\begin{aligned} f'_{1,i} &= 2\mathcal{X}_{c,i} \Big[\lambda_1 (\hat{I}_{2x,i} \hat{I}_{2xx,i} + \hat{I}_{2y,i} \hat{I}_{2xy,i}) + \lambda_2 (\hat{I}_{2,i} - I_{2,i})(\hat{I}_{2x,i} - I_{2x,i}) \\ &\quad + \lambda_3 \alpha (\alpha \hat{I}_{2,i} + \beta - I_{1,i}) \hat{I}_{2x,i} \Big] \\ f'_{2,i} &= 2\mathcal{X}_{c,i} \Big[\lambda_1 (\hat{I}_{2x,i} \hat{I}_{2xy,i} + \hat{I}_{2y,i} \hat{I}_{2yy,i}) + \lambda_2 (\hat{I}_{2,i} - I_{2,i})(\hat{I}_{2y,i} - I_{2y,i}) \\ &\quad + \lambda_3 \alpha (\alpha \hat{I}_{2,i} + \beta - I_{1,i}) \hat{I}_{2y,i} \Big] \end{aligned}$$

$$
\begin{aligned}
K_{11,i} &= 2\mathcal{X}_{c,i}\Big[\lambda_1(\hat{I}^2_{2xx,i}+\hat{I}^2_{2xy,i})+\lambda_2(\hat{I}_{2,i}-I_{2,i})(\hat{I}_{2xx,i}-I_{2xx,i}) \\
&\quad+\lambda_2(\hat{I}_{2x,i}-I_{2x,i})^2+\lambda_3\alpha(\alpha\hat{I}_{2,i}+\beta-I_{1,i})\hat{I}_{2xx,i}+\lambda_3\alpha^2\hat{I}^2_{2x,i}\Big] \\
K_{12,i} &= 2\mathcal{X}_{c,i}\Big[\lambda_1(\hat{I}_{2xy,i}\hat{I}_{2xx,i}+\hat{I}_{2xy,i}\hat{I}_{2yy,i})+\lambda_2(\hat{I}_{2,i}-I_{2,i})(\hat{I}_{2xy,i}-I_{2xy,i}) \\
&\quad+\lambda_2(\hat{I}_{2x,i}-I_{2x,i})(\hat{I}_{2y,i}-I_{2y,i})+\lambda_3\alpha(\alpha\hat{I}_{2,i}+\beta-I_{1,i})\hat{I}_{2xy,i}+\lambda_3\alpha^2\hat{I}_{2x,i}\hat{I}_{2y,i}\Big] \\
K_{22,i} &= 2\mathcal{X}_{c,i}\Big[\lambda_1(\hat{I}^2_{2xy,i}+\hat{I}^2_{2yy,i})+\lambda_2(\hat{I}_{2,i}-I_{2,i})(\hat{I}_{2yy,i}-I_{2yy,i}) \\
&\quad+\lambda_2(\hat{I}_{2y,i}-I_{2y,i})^2+\lambda_3\alpha(\alpha\hat{I}_{2,i}+\beta-I_{1,i})\hat{I}_{2yy,i}+\lambda_3\alpha^2\hat{I}^2_{2y,i}\Big] \qquad (9)
\end{aligned}
$$

$\mathbf{K}_{13}$ and $\mathbf{K}_{23} \in R^{n\times 2}$, and the i-th element in the first and second columns of each of these matrices are denoted by $K_{13,1,i}$, $K_{13,2,i}$, $K_{23,1,i}$ and $K_{23,2,i}$ respectively. These values are presented as:

$$
\begin{aligned}
K_{13,1,i} &= 2\lambda_3\mathcal{X}_{c,i}(2\alpha\hat{I}_{2,i}+\beta-I_{1,i})\hat{I}_{2x,i} \\
K_{13,2,i} &= 2\lambda_3\mathcal{X}_{c,i}\alpha\hat{I}_{2x,i} \\
K_{23,1,i} &= 2\lambda_3\mathcal{X}_{c,i}(2\alpha\hat{I}_{2,i}+\beta-I_{1,i})\hat{I}_{2y,i} \\
K_{23,2,i} &= 2\lambda_3\mathcal{X}_{c,i}\alpha\hat{I}_{2y,i} \qquad (10)
\end{aligned}
$$

f'_α and f'_β are scalar values, $\mathbf{K}_{33}$ is a 2×2 matrix, they are specified as:

$$
\begin{aligned}
f'_\alpha &= 2\lambda_3\sum_i \mathcal{X}_{c,i}\hat{I}_{2,i}(\alpha\hat{I}_{2,i}+\beta-I_{1,i}) \\
f'_\beta &= 2\lambda_3\sum_i \mathcal{X}_{c,i}(\alpha\hat{I}_{2,i}+\beta-I_{1,i}) \\
\mathbf{K}_{33} &= 2\lambda_3\begin{bmatrix}\sum_i \mathcal{X}_{c,i}\hat{I}^2_{2,i} & \sum_i \mathcal{X}_{c,i}\hat{I}_{2,i} \\ \sum_i \mathcal{X}_{c,i}\hat{I}_{2,i} & \sum_i \mathcal{X}_{c,i}\end{bmatrix} \qquad (11)
\end{aligned}
$$

In the above two equations, all values related to $\hat{I}_2$ and I_2 are computed at $(x_i+v_{1,i}, y_i+v_{2,i})$, which can be computed using any interpolation techniques. And all values related to I_1 are computed at (x_i, y_i). Note that the second-order partial derivatives of the discretized energy function, $K_{11,i}$, $K_{12,i}$, $K_{22,i}$ are obtained by ignoring the terms involving third-order partial derivatives, which are more sensitive to the high-frequency noise.

4 Implementation Results

In this section, we present several examples of application of our algorithm to achieve registration and segmentation. Results of this application are presented for synthetic as well as real data in 2D. We present one synthetic and three real data examples. The synthetic data example contains a synthetically generated source image and a target image which was generated from the source image by a known non-rigid field that was procedurally generated. In this case, we present

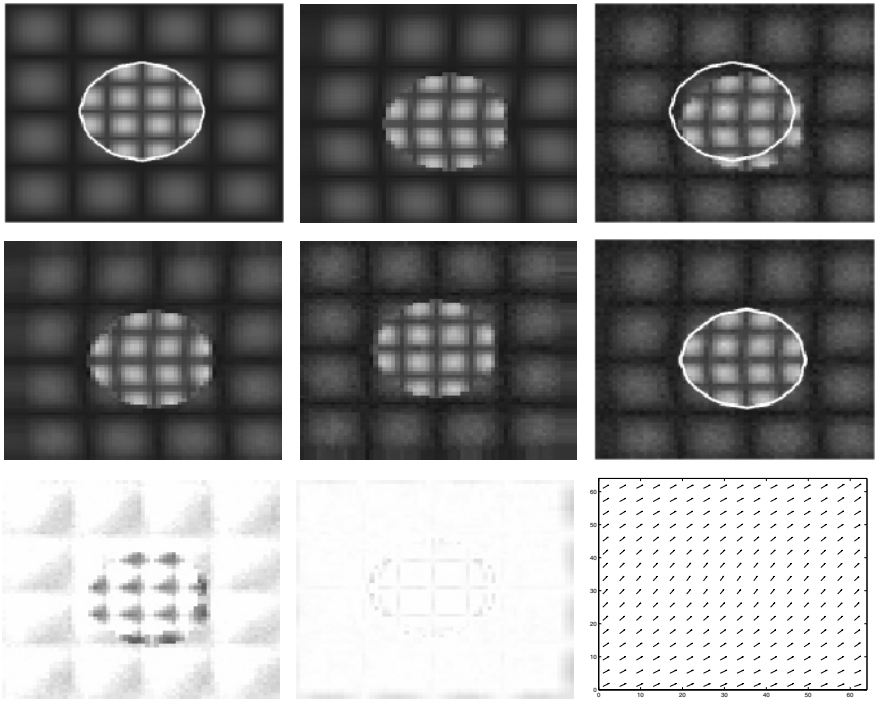

Fig. 1. Results of application of our algorithm to synthetic data (see text for details).

the error in the estimated non-rigid field using our algorithm as an indication of the accuracy of the algorithm.

The segmentations in all the examples that are to be used as the "atlas" segmentation was semi-automatically estimated using an active contour model. More sophisticated methods involving use of statistical information outlined in literature discussed in section 1 can be used to create these atlas-segmentations and we will use such methods in our future work. All the figures are organized as follows, from left to right: the first row depicts the source image with the atlas-segmentation superposed in white, the target image which is to be segmented followed by the target image with the unregistered atlas-segmentation superposed to depict the amount of mis-alignment; second row depicts smoothed target, registered target followed by the segmented and registered target; third row depicts the difference between the source and the unregistered target to show the degree of discrepancy between the unregistered image pairs followed by the difference between them after registration and finally the estimated non-rigid vector field.

Figure 1 depicts the results obtained for the noisy synthetic data. The source image was generated with sufficient texture in the region of interest. The target was then obtained by applying a synthetically generated non-rigid deformation

field to the source image. The results are organized as described earlier. As evident, the registration+smoothing+segmentation are quite accurate from a visual inspection point of view. As a measure of accuracy of our method, we estimated the average and the standard deviation of the error in the estimated non-rigid deformation field. The error was estimated as the angle between the ground truth and estimated displacement vectors. The average and standard deviation are, 1.8742 and 4.5061 (in degrees) respectively, which is quite accurate.

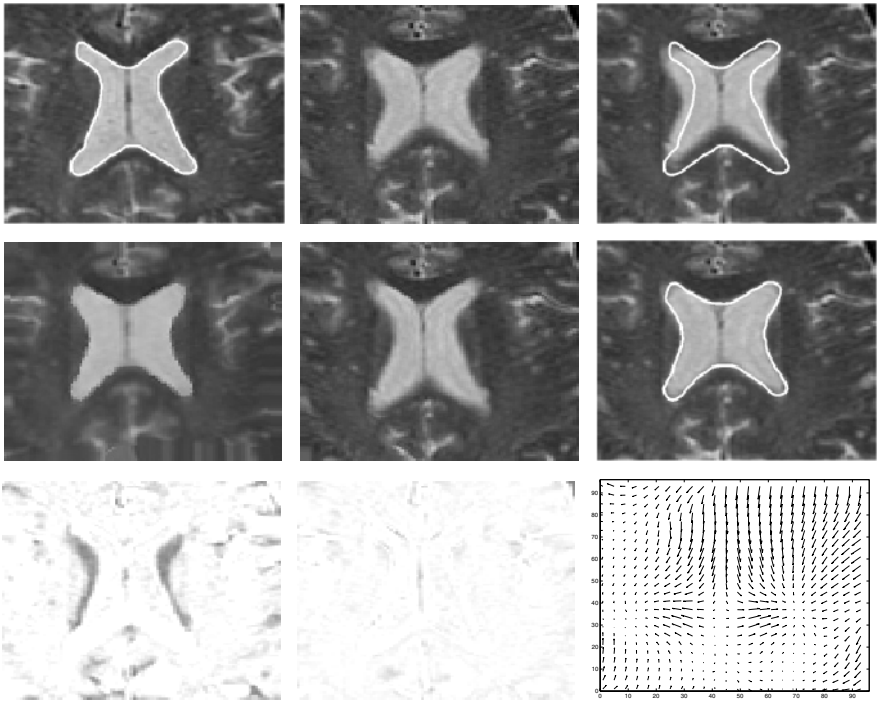

Fig. 2. Results of application of our algorithm to a pair of slices from a human brain MRI (see text for details).

For each of the first two real data experiments, we selected two image slices that were two slices apart from an MR brain data set. The two slices depict considerable changes in shape of the ventricles, the region of interest in the data sets. One of the two slices was arbitrarily selected as the source and segmentation of the ventricle in the source was achieved using an active contour model. The goal was then to automatically find the ventricle in the target image using our algorithm given the input data along with the segmented ventricles in the source image. The results as organized as before. As evident from figures 2 and 3, the accuracy of the achieved registration+segmentation visually very good. Note

that the non-rigid deformation between the two images in these two examples is quite large and our method was able to simultaneously register and segment the target data sets quite accurately.

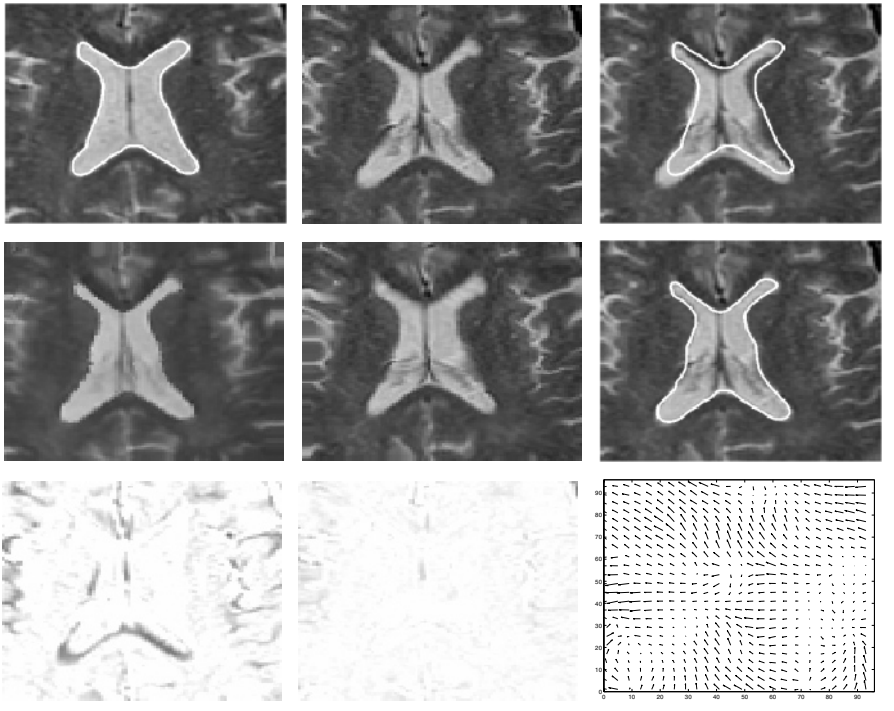

Fig. 3. Results of application of our algorithm to another pair of slices from a human brain MRI (see text for details).

Finally, the last real data example is obtained from two brain MRIs of different subjects and the segmentation of the cerebellum in the source image is given. We selected two "corresponding" slices from these volume data sets to conduct the experiment. Note that even though the number of slices for the two data sets are the same, the slices may not correspond to each other from an anatomical point of view. However, for the purposes of illustration of our algorithm, this is not very crucial. We use the corresponding slice of the 3D segmentation of the source as our atlas-segmentation. The results of an application of our algorithm are organized as before. Once again, as evident, the visual quality of the segmentation and registration are very high. In the first experiments, the parameter values used in our model are: $\lambda_1 = 0.1, \lambda_2 = \lambda_3 = 1, \lambda_4 = 0.2$, for the rest of the experiments, we use: $\lambda_1 = 0.2, \lambda_2 = \lambda_3 = 1, \lambda_4 = 0.4$.

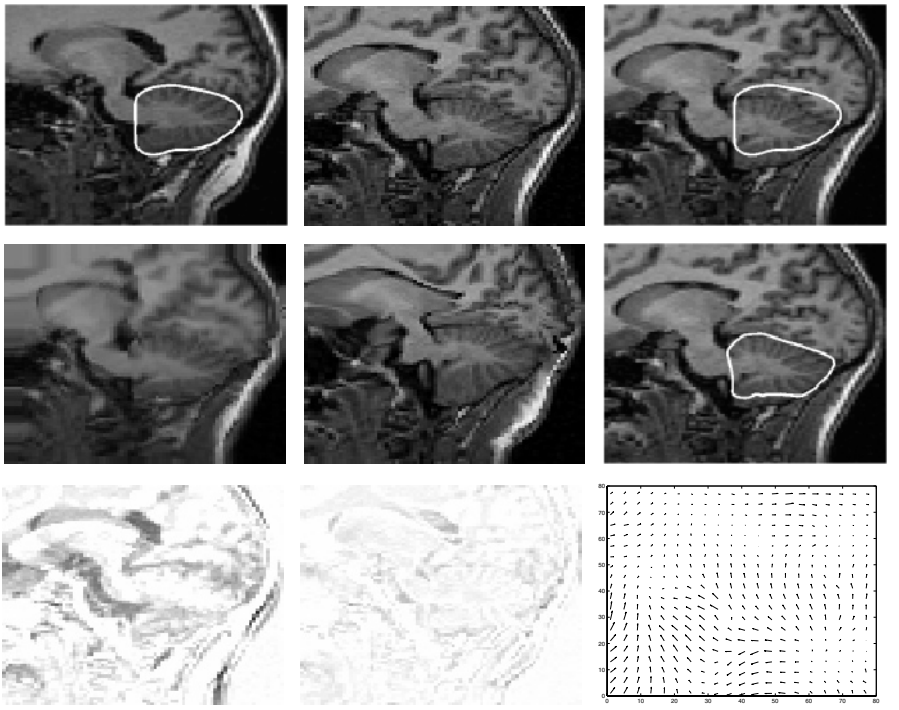

Fig. 4. Results of application of our algorithm to a pair of corresponding slices from distinct subjects.(see text for details)

5 Conclusions

Image segmentation is a fundamental problem in Image Processing, Computer Vision and Medical Imaging with numerous applications. There are numerous existing methods in literature for achieving this goal. One of the most successful scheme for achieving image segmentation in Medical Imaging has been atlas-based or model-based methods. We dub this a registration assisted segmentation scheme because the atlas-segmentation is non-rigidly registered to the target. In this paper, we present a novel variational formulation of this registration assisted image segmentation problem which leads to solving a coupled set of nonlinear PDEs that are solved using efficient numerical schemes. Our work is a departure from earlier methods in that we have a *unified variational principle* wherein registration and segmentation are simultaneously achieved. We presented several 2D examples on synthetic and real data sets along with quantitative accuracy estimates of the registration in the synthetic data case. More extensive experimentation under different amounts of noise and varying degrees of non-rigidity needs to be performed prior to drawing conclusions on the accuracy of the proposed model. This will be the focus of our future efforts.

References

1. L. Zollei A. Yezzi and T.Kapur. A variational framework for joint segmentation and registration. In *IEEE Workshop on Biomedical Image Analysis*, pages 44–51, Kauai, Hawaii, 2001.
2. Y.Chen B. Vemuri, J. Ye and C.Leonard. A level-set based approach to image registration. In *IEEE Workshop on Biomedical Image Analysis*, pages 86–93, Hilton Head Island, SC, 2000.
3. M. Chen, T. Kanade, H. A. Rowley, and D. Pomerleau. Quantitative study of brain anatomy. In *IEEE Workshop on Biomedical Image Analysis*, pages 84–92, Santa Barbara, CA, 1998.
4. Sarang C.Joshi, Ayananshu Banerjee, Gary E.Christensen, John G.Csernansky, John W.Haller, Michael I.Miller, and Lei Wang. Gaussian random fields on submanifolds for characterizing brain surfaces. In *15th International Conference, IPMI'97*, Poultney, Vermont, June 1997.
5. A. Collignon, F. Maes, D. Vandermeulen, P. Suetens, and G. Marchal. Automated multimodality image registration using information theory. In *Info. Processing in Medical Images*, pages 263–274, Brest, France, 1995.
6. B. M. Dawant, S. L. Hartmann, J. P. Thirion, F. Maes, D. Vandermeulen, and P. Demaerel. Automatic 3-d segmentation of internal structures of the head in mr images using a combination of similarity and free-form transformations: Part i, methodology and validation on normal subjects. *IEEE Trans. on Medical Imaging*, 18(10):909–916, 1999.
7. D.Rueckert, A. F. Frangi, and J. A. Schnabel. Automatic construction of 3d statistical deformation models using non-rigid registration. In *Fourth International Conference, MICCAI 2001*, Utrecht, The Netherlands, October 2001.
8. G. E.Christensen, M. I. Miller, and M. Vannier. Individualizing neuroanatomical atlases using a massively parallel computer. *IEEE Computer*, 1(29):32–38, 1996.
9. C. Meyer et. al. Demonstration of accuracy and clinical versatility of mutual information for automatic multimodality image fusion using affine and thin-plate spline-warped geometric deformations. *Medical Image Analysis*, 1:195–206, 1997.
10. Guido Gerig, Martin Styner, Martha E.Shenton, and Jeffrey A.Lieberman. Shape versus size: Improved understanding of the morphology of brain structures. In *Fourth International Conference, MICCAI 2001*, Utrecht, The Netherlands, October 2001.
11. Nikos Paragios and Rachid Deriche. Corrections to 'geodesic active contours and level sets for the detection and tracking of moving objects'. *IEEE Trans. on Pattern Analysis and Machine Intelligence*, 22(4):415, Apr. 2000.
12. W. Murray P.E. Gill and M.H. Wright. *Practical Optimization*. Academic Press, London, New York, 1981.
13. D. Rueckert, L. I. Sonda, D.L. G. Hill C. Hayes, M. O. Leach, and D. J. Hawkes. Nonrigid registration using free-form deformations: Application to breast mr images. *IEEE Trans. on Medical Imaging*, 18(8):712–721, 1999.
14. Yousef Sadd. *Iterative Methods for Sparse Linear Systems*. PWS Publishing Company, Boston, MA, 1995.
15. T. Schormann, S. Henn, and K. Zilles. A new approach to fast elastic alignment with application to human brains. In *Visualization in Biomedical Computing*, pages 338–342, Hamburg, 1996.
16. J.R. Shewchuk. An introduction to the conjugate gradient method without the agonising pain. Technical Report CMU-CS-94-125, Carnegie Mellon University, School of Computer Science, Mar. 1994.

17. R. Szeliski and J. Coughlan. Hierarchical spline-based image registration. In *IEEE Conf. Comput. Vision Patt. Recog*, pages 194–201, Seattle, 1994.
18. P. Thevenaz and M. Unser. Optimization of mutual information for multiresolution image registration. *IEEE Trans. on Image Processing*, 9(12):2083–2099, Dec. 2000.
19. J. P. Thirion. Image matching as a diffusion process: an analogy with maxwell's demons. *Medical Image Analysis*, 2(3):243–260, 1998.
20. A. Trouve. Diffeomorphisms groups and pattern matching in image analysis. *International Journal of Computer Vision*, 28(3):213–221, 1998.
21. Andy Tsai, Jr. A. Yezzi, and Alan S. Willsky. Curve evolution implementation of the mumford-shah functional for image segmentation, denoising, interpolation, and magnification. *IEEE Trans. on Image Processing*, 10(8):1169–1186, Aug. 2001.
22. P. Viola and W. M. Wells III. Alignment by maximization of mutual information. In *Intl. Conf. on Compu. Vision*, pages 16–23, Cambridge, MA, 1995.
23. Y. Wang and L. H. Staib. Elastic model based non-rigid registration incorporating statistical shape information. In *Medical Image Computing and Computer-Assisted Intervention*, pages 1162–1173, Boston, MA, Oct. 1998.